A Runge-Kutta Approach to Probing the Structure of White Dwarf Stars

A. A. Lascelles
School of Physics and Astronomy
University of Southampton
SO17 1BJ
United Kingdom
E-mail: aal1g13@soton.ac.uk

March 20, 2016

Abstract

A model for determining mass-radius variation for white dwarfs with a relativistic free Fermi gas equation of state is investigated. Under this model, a density profile for a single white dwarf is constructed. Both theoretical parameters from an SDSS white dwarf search and observational parameters from Sirius B, 40 Eri B, Stein 2051, and Procyon B are found to be consistent with the predictions of the model. The functional form of the mass-radius relation is tested for both He/C/Mg and Fe core white dwarfs under relativistic, non-relativistic and extremely-relativistic regimes. Ultimately, the Chandrasekhar mass is obtained for He/C/Mg and Fe core WDs with values of $1.44 \pm 2.22^{-10} M_{\odot}$ and $1.24 \pm 2.22^{-10} M_{\odot}$ respectively.

1. Introduction

Accurate understanding of the inner workings of white dwarf (WD) stars is of great importance for many branches of astronomy, including galaxy formation, stellar evolution, and supernovae studies. Since over 95% of stars we observe will end their lives as WDs[1], knowing how they function is crucial and by studying them, we are able to study the history of the progenitor main sequence star. They are our testing grounds for matter undergoing extreme physical processes near the end of a star's lifetime. This paper presents how their masses are related to their radii, which is considered the primary focus of this work. Currently, complex models take into account factors such as atmospheric conditions, magnetic fields, and pulsations. They accurately pinpoint the relation between mass, radius, density, and temperature for sub-classes of WDs. This paper aims to arrive at the same conclusions using a more basic degenerate free Fermi gas model.

WDs are formed when low to mid-mass ($< 8M_{\odot}$) stars have used up all of their nuclear fuel through fusion processes, converting H and He to C, Si and in some cases Fe. Expanding by almost one hundred-fold, they may become an object known as a red giant. They shed their outer layers which form planetary nebulae and leave behind their cores. They must undergo mass-loss processes, such as stellar winds, to end up with average masses of $0.6M_{\odot}$[1] equating to radii on scales similar to that of planet Earth. With fusion out of the picture, WDs have no source of outward radiation pressure but due to their mass they still feel inward gravitational forces. It can easily be seen that some outward pressure is needed to balance this, or else all stars would inevitably collapse in on themselves. The solution is that WDs are supported by electron degeneracy pressure. Such a force stops free electrons from being compressed so close to nuclei that they would occupy the same energy state and violate Pauli's exclusion principle[2]. It has been shown that electron degeneracy pressure could produce a strong enough repulsive force to support a WD against the inwards gravitational force. As electrons are pushed closer towards the nuclei, they fall into lower and lower energy levels, decreasing their energy which, combined with what is known about their small radii, explains their observed low luminosities ($\sim 10^{-4}$ to $10^{-2}L_{\odot}$)[3]. At this stage, the WDs have nothing else to do but cool down until they end their lives as a theorised black dwarf. Due to the large thermal timescales, this cooling process will last longer than the current age of the universe. A brown dwarf, on the other hand, is different object that becomes non-relativistic too early on in it's evolution that it never fuses H. Characterised by their low luminosities and spectral lines from their chemical composition, they differ greatly from white dwarfs which have evolved past H fusion before collapse.

There is, however, a limit in which the degeneracy pressure breaks down and the mass becomes too large to counteract. At these masses, the star will collapse further into a neutron star or black hole. Chandrasekhar showed in the early 1930s that when an electron degenerate gas is allowed to act relativistically, this mass limit is $M_{Ch} = 1.44M_{\odot}$[4].

Depending on the seed star and the environment history, varying core compositions can be produced - in this paper both He/C/Mg and Fe core WDs are considered (from this point onwards, He/C/Mg cores will be referred to as C cores due to their identical number of electrons per nucleon). It is common to have a C-O core surrounded by a He envelope which is also encapsulated by a thinner H envelope. Some observed WDs have a lower radius than expected suggesting an Fe core. The ultimate fate of most WDs is to cool slowly and redden for lengths of time longer than the current age of the universe. If however, there is a companion star, then in this binary system the WD can accrete matter until it exceeds the M_{Ch} and a type 1a supernova is produced. In some cases, after a failed supernova explosion, some of the products can be reabsorbed, with Fe and other metals accumulating in the core. Such a method is a recent proposal to the progenitor of the Fe core WDs that we observe[5]. Other explanations include a binary system in which a massive main sequence star is stripped of its outer layers to leave behind an Fe core.

In section 2, we present an overview of the methods used, both mathematical manipulation and computational inputs, to allow the problem to be solved. Section 3 gives a full discussion of the results and the physical interpretations of them. The findings will be summarised in section 4, with any full derivations available to view in the appendices.

2. Methodology

The implementation of the method is twofold and documented within the following sub-sections. Firstly a non-dimensionalisation of the differential equations relating pressure, density, mass, and radius of a star into a form that could be used to solve the problem computationally. This requires a definition of dimensionless variables and substitution technique to output two first order differential equations. Secondly, correct usage and understanding of the Runge-Kutta algorithm is needed to integrate these differential equations outwards and graphically present the solutions in such a way to verify the mass and density of known WDs such as Sirius B. Our model is calculated on the assumption of our WD, with its structure described by a relativistic free Fermi gas, being spherically symmetric and in hydrostatic equilibrium. The exact details of these methods are discussed in the following subsections. However, before this, the Runge-Kutta numerical method must be tested. This is done with a simple problem involving a hanging chain undergoing simple harmonic motion, described by a set of differential equations. Using the boundary conditions, the stable states of this system are found and compared to documented values, confirming the validity of the numerical method to be used.

2.1. Manipulation of Differential Equations

WD stars are complex objects with intrinsic properties that change on small scales from the core to the surface, and as such must be described by differential rather than regular linear equations. Mass is the main parameter determining the properties of stars and so it is important to know how it changes within a given star. Variation in mass depends on density, ρ, which in turn varies with pressure.

The first important differential equation is a statement of $\rho = \frac{m}{V}$ for infinitesimal changes in mass, m, and radius, r:

$$\frac{dm}{dr} = 4\pi r^2 \rho. \tag{1}$$

Our second important differential equation determines the variation of density with radius and is a function of mass, radius, and pressure, P:

$$\frac{d\rho}{dr} = -\left(\frac{dP}{d\rho}\right)^{-1} \frac{Gm}{r^2}\rho, \tag{2}$$

where G is the gravitational constant. This differential in turn depends on another differential involving pressure, a γ factor, and Y_e, the number of electrons per nucleon. It is called the equation of state and it can be shown (see Appendix A) that matter within a WD can be well approximated as a relativistic free Fermi gas which takes the following form:

$$\frac{dP}{d\rho} = Y_e \frac{m_e c^2}{m_p} \gamma\left(\frac{\rho}{\rho_0}\right), \tag{3}$$

where m_p and m_e are the masses of a proton and electron respectively and the gamma function is given by,

$$\gamma(y) = \frac{y^{\frac{2}{3}}}{3(1 + y^{\frac{2}{3}})^{\frac{1}{2}}}. \tag{4}$$

The manipulation of these equations for computational use involves the definition of dimensionless quantities M, q, and x which act to non-dimensionalise mass, density, and radius respectively:

$$M = \frac{m}{\frac{4}{3}\pi R_0^3 \rho_0}, \tag{5}$$

$$q = \frac{\rho}{\rho_0}, \tag{6}$$

$$x = \frac{r}{R_0}, \tag{7}$$

such that these variables only vary from 0 to 1. This step is important as very large or small numbers often cause the incorrect evaluation of equations within computational programs.

Upon substitution of (5) and (6) into (1) we arrive at the dimensionless differential equation below.

$$\boxed{\frac{dM}{dx} = 3x^2 q} \tag{8}$$

Similarly, after substitution of (5), (6), and (7) into (2), rearrangement yields the second important differential equation:

$$\boxed{\frac{dq}{dx} = -C\frac{qM}{x^2\gamma(q)},} \tag{9}$$

where the constant $C \approx 0.86$ and is given by,

$$C = \frac{4\pi G R_0^2 \rho_0 m_p}{3Y_e m_e c^2}. \tag{10}$$

The two boxed equations (9) and (10) are the forms of the equations fed to the Runge-Kutta algorithm detailed in the subsequent section.

2.2. Runge-Kutta Method

A fourth-order Runge-Kutta algorithm is used to solve equations (8) and (9). All equations mentioned are input using a number of functions and the constant C is absorbed by redefinition of the dimensionless variables. An additional boundary condition of $\frac{\rho}{\rho_0} = 0$ when $x = 0$ is added such that density is only non-zero for systems with a physical size. Once this is established, the density profile can be plotted by cycling through the two Y_e values for Fe and C cores. In order to have a good balance between the required high accuracy and the computational time, the number of iterations is set at $N = 10^3$ for medium densities and $N = 10^6$ for the lowest/highest densities where the boundary conditions are approached. In order to reduce the error in the Runge-Kutta method due to truncation, this number of iterations is chosen in accordance with guidance from Numerical Methods MATH3018[6]. Boundary conditions for the Runge-Kutta algorithm are set as $x = 0$, $M = 0$ and $q = 1$ and while the value of the density is larger than a very small value ($q > 10^{-10}$) the program is allowed to run. This small value is chosen such that the second boundary condition of the density at the WD's surface tending to zero is implemented as 10^{-10} can be justifiably approximated as zero. The values of x and q are recovered, and hence the relationship between radius and density plotted.

In addition to this density profile, a relationship between mass and radius for any WD, constrained to this model's assumptions, is then found. This is achieved by defining a list of core densities, ρ_c, which could be looped over for each solution of the set of equations. The boundary conditions remained the same apart from the change of density to $q = \rho_c$. When each core density calculation terminates, signalling the reaching of a boundary condition, the final value is recorded and the respective mass added to an array and converted to solar units. With these values, the variation of mass with radius can finally be plotted. In order to verify the model with observation, data points for three WD sources are overlaid, with their error bars indicating the success of the model to simulate real physical conditions.

3. Results and Discussion

3.1. Relativistic Case

We set out to compare our model to data points for the four WDs listed in Table 1 in order to check its validity. There is limited documentation on the mass *and* radius of white dwarfs as they are faint objects which requires them to be in a binary system nearby to get independent parameters which is rare. However, Sirius B, 40 Eri B, Stein 2051, and Procyon B are well documented enough by man separate telescope observations to have reliable masses/radii, and as such are perfect candidates.

White Dwarf	Mass/$M_\odot$	Radius/$R_\odot$
Sirius B	1.053±0.028	0.0074±0.0006
40 Eri B	0.48±0.02	0.0124±0.0005
Stein 2051	0.50±0.05	0.0115±0.00012
Procyon B	0.602±0.015	0.01234±0.00032

Table 1: Raw data for the mass and radius of the four WDs used in this project: Sirius B, 40 Eri B, Stein 2051, and Procyon B[7]. Solar masses/radii is the preferred unit of choice.

To begin with, the density (as the dimensionless quantity $\frac{\rho}{\rho_0}$) is plotted against radius for a single WD - illustrated in Fig. 1. It is seen that the composition of the core makes a small but noticeable change to the profile. Fe cores become less dense more quickly when moving out radially from the centre, suggesting that more mass is enclosed within

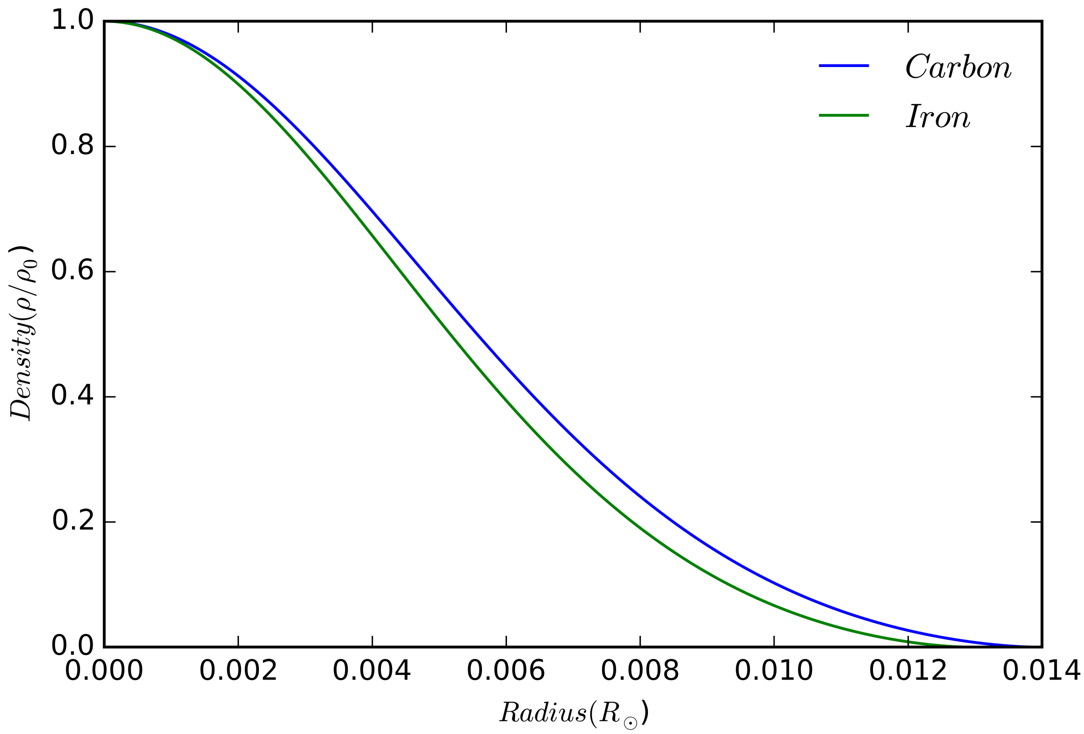

Figure 1: Density profile for an Fe and C core WD under a relativistic free Fermi gas equation of state model.

a smaller radius. In normal stars this would result in a higher temperature however WD's temperature dependence, being degenerate, has no effect on any of the other physical properties of the star. The density decays with radius faster for Fe core resulting in a smaller final radius. The maximum radius allowed by our model is $0.0139 \pm 2.22^{-10} R_\odot$ for Fe cores and $0.0129 \pm 2.22^{-10} R_\odot$ for C cores, signifying that the size of WDs is on the same scale as the radius of planet Earth. The relationship between density and radius is almost linear for the middle portion of the star whilst near the core and surface it drops off faster following a power law.

Using the method illustrated in section 2.2 and further detailed in Appendix D, a plot of mass against radius is constructed for both C and Fe core WDs. It is found that Sirius B and Procyon B fitted best to the C core model whilst Stein 2051 and 40 Eri B fell within a Fe core model (see Fig. 2). A possible explanation of these Fe core WDs are that the objects are initially high mass stars fusing up to Fe in their cores which have their outer shells stripped away by accretion from a binary companion star.

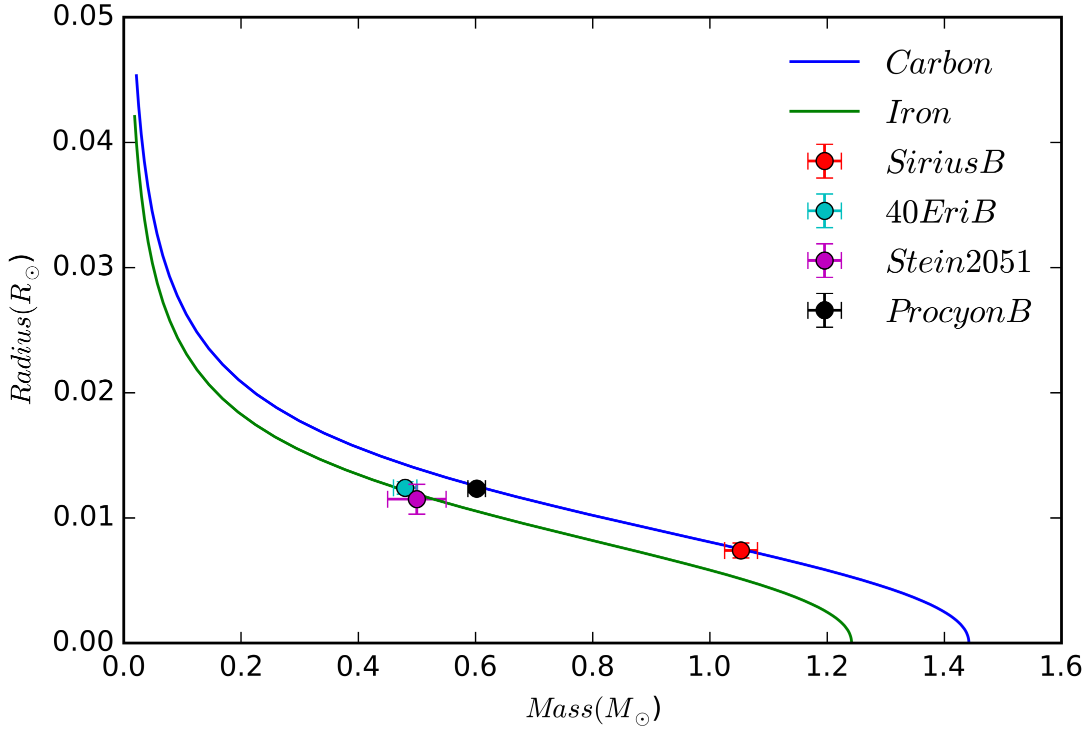

Figure 2: Variation of WD mass with radius. Experimental data points with error bars for known sources are overlaid showing their agreement with the theoretical model. The expected Chandrasekhar mass of $1.44M_\odot$ is recovered in the C core case. WD data points obtained from Provencal et al.[7] and the project notes.[4] [8] [9]

Counterintuitively to regular stellar evolution, it is shown in Fig. 2 that as mass increases WD radius *decreases*. This can be explained by a larger gravitational force compared to a relatively equal electron degeneracy pressure, whereas in regular stars a larger mass would create a larger radius. This process happens up until a certain point called the Chandrasekhar mass limit, M_{Ch}, where the electron degeneracy pressure can no longer withstand the gravitational force and the WD would trigger a type 1a supernova or become a neutron star/black hole if its history always consisted of a mass, $M > M_{Ch}$. The following paragraphs will detail the results displayed in Fig. 2 and discuss their significance.

Because mass is the most important variable when determining physical effects in any star, it has been plotted on the x-axis. In the low mass regime, the curve can be described as ideal gas pressure dominated with a high power law representing the fast drop-off. When the slope levels out at masses of $\sim 0.4M_\odot$ we enter the near-relativistic degenerate gas regime which has an equation of state giving gradient equal to $-\frac{1}{3}$, $P \sim \rho^{5/3}$, and polytropic index of $\frac{3}{2}$. It is in this regime that that our data points lie which is expected since the previously mentioned average mass is $0.6M_{\odot}$ with most WDs falling between $0.5M_{\odot}$ to $0.8M_{\odot}$. This curve deviates as we enter the extremely relativistic degenerate gas regime where the radius decreases quickly to a critical mass, M_{Ch}. Including error analysis of the Runge-Kutta method[10], it is found that the mass limit is $1.44 \pm 2.22^{-10}M_{\odot}$ for Fe core and $1.24 \pm 2.22^{-10}M_{\odot}$ for C core WDs which is in agreement with theory[4]. This result is very significant as it sets the maximum mass of WDs.

3.2 Extension

3.2.1 SDSS Data

In order to verify our model further, 20 WD data points are found in the SDSS Data Release 1[11] and plotted alongside the observational data discussed previously. It can be seen that considering the appropriate error bars, they fall within the constraints of the model and act positively to re-enforce the validity of this study.

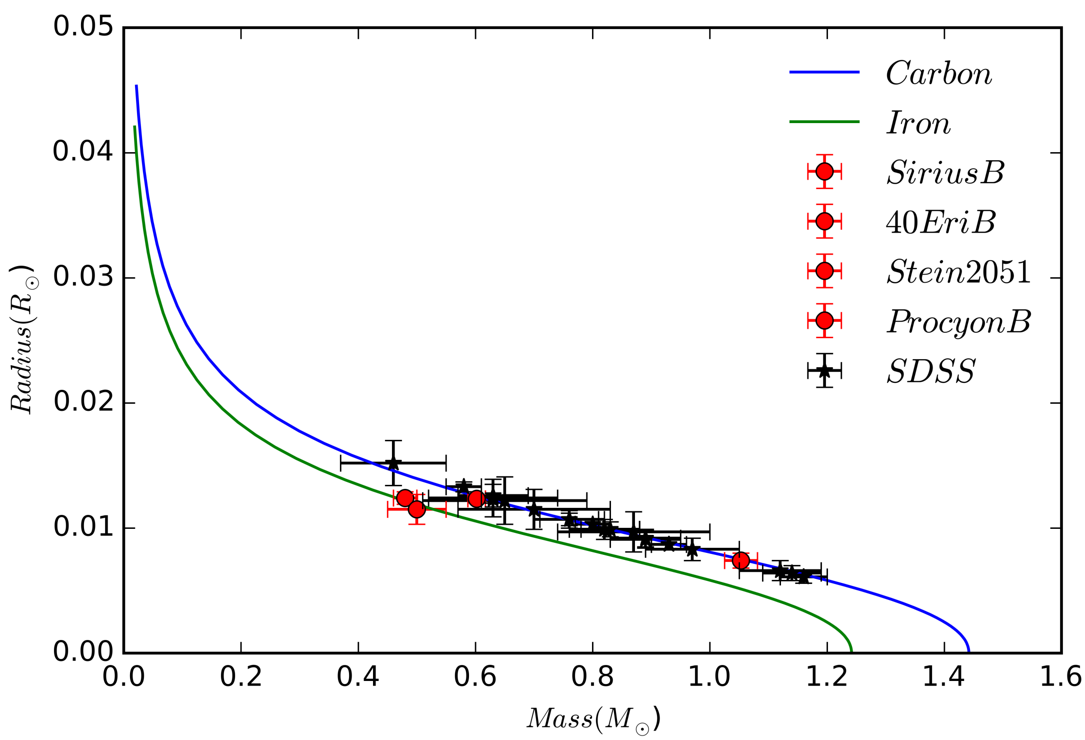

Figure 3: 20 additional data points from SDSS[11] included in the original plot to further verify the model. Plotted in red are the 4 well documented WDs as comparison.

3.2.2 Non-Relativistic and Extremely Relativistic Cases

For completeness, non-relativistic and extremely relativistic cases are investigated using the methods outlined in Appendices B and C. As seen in Fig. 4, the extremely relativistic case (where velocity is equal to the speed of light) represents the limit at the Chandrasekhar mass and is a straight vertical line at this value. The non-relativistic case begins the same as the relativistic case at low masses. However, at $0.2M_{\odot}$ it deviates from the relativistic case and extends past the Chandrasekhar masses as it slowly tends to zero. It can therefore be seen that the correct form of the gas to explain WDs is the relativistic case.

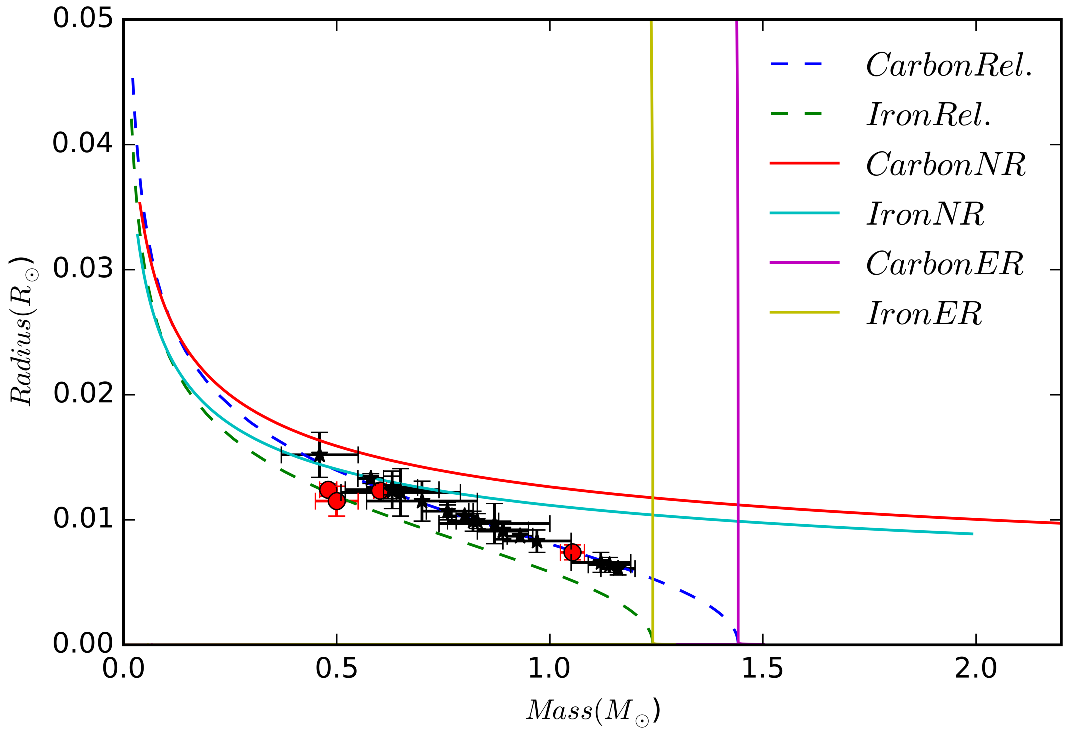

Figure 4: Non-relativistic and extremely relativistic Fermi gas cases plotted alongside the relativistic case. The best description of WDs comes from the relativistic case.

3.3 Additional Research and Limitations

Further extensions of this project could involve probing the regime past the mass limit where the star ceases to be a WD. Beyond the Chandrasekhar mass (shown in Fig. 2) a WD has one of three possible outcomes[12] which all depend on the balance between the degeneracy pressure, P_{deg}, and the pressure due to gravity, P_g. The first of these scenarios is accretion from a red giant/main sequence companion leading to a type 1a supernova. High redshift measurements rely on this standardisable candle. Secondly, the pressure balance could be disturbed by a collision between two nearby WDs, causing the less massive one to be torn apart by tidal forces whilst the other collapses before thermonuclear runaway. Lastly, He in the outer envelope of a C-O WD may suddenly undergo fusion to C/O sending a shock wave which causes $P_g > P_{deg}$ and an ignition in the core.

Taking into account the rotation of WDs may affect the observed mass-radius relation. This effect, being a current area of research[13], is not fully understood but is believed to be the cause of variation in luminosity and masses above the Chandrasekhar limit. Either rigid (lower mass) or differential (higher mass) rotation could be investigated to see how the mass-radius relation is altered. These bodies are known to pulsate in some cases - changing the mass-radius relation further.

WD cooling processes and cosmochronology could also be investigated[14]. WDs tend to have very long thermal timescales meaning their lifetimes are incredibly long. As there is no fusion occurring, they slowly radiate away their energy and cool down to eventually form an object known as a black dwarf. Black dwarfs have never been observed due to this large thermal timescale, but it is well within the scope of a further research project to study the effect of cooling on WDs. Additionally, the magnetic fields of such WDs have been neglected here and undoubtedly change the mass/radius.

Another possible area of further research is the inclusion of a density function that changes from core to surface to accurately describe the different regions in a WD. Besides the core, there are also thin envelopes of H and He which alter the physics of the system.

This project is limited by the lack of observational data points to compare the model to. Although the four chosen to investigate and the theoretically calculated mass/radii values from SDSS had uncertainties that fell within the range of our model, pure first-hand observationally confirmed masses/radii are missing. To thoroughly conclude the correctness of this model, more comparisons are necessary. The assumptions that He/C/Mg core WDs are identical because of their Y_e values and that we can ignore the outer envelopes are incorrect thus can be seen as limitations. One cannot properly describe the mass-relation without differentiating between He/C/Mg cores and including the effect of a thin envelope.

4. Conclusion

A model based on a relativistic free Fermi gas is constructed and tested for observational data from 4 WDs and theoretical data for 20 WDs from the SDSS Data Release. Using a fourth-order Runge-Kutta approach, parameters such as density, radius, and mass are found computationally and plotted with the above mentioned points overlaid for comparison. The resulting graphs for density against radius for a single WD and mass against radius for all WDs re-confirms the underlying theory outlined in the introduction. Using a simplified approach, the Chandrasekhar mass and functional form for He/C/Mg and Fe core WDs is obtained, yielding $1.44 \pm 2.22^{-10} M_{\odot}$ and $1.24 \pm 2.22^{-10} M_{\odot}$ respectively, matching previously documented values. Non-relativistic and extremely-relativistic limits are also tested concluding that WDs are best described under the relativistic degenerate gas regime.

Appendix A: Relativistic Case

Within this appendix, under the assumption of a near relativistic gas, the derivation of the equation of state used for this model is presented[15]. We aim to prove:

$$\frac{dP}{d\rho} = Y_e \frac{m_e c^2}{m_p} \gamma\left(\frac{\rho}{\rho_0}\right),$$

where,

$$\gamma(y) = \frac{y^{\frac{2}{3}}}{3(1 + y^{\frac{2}{3}})^{\frac{1}{2}}}.$$

The equation for pressure of our gas is,

$$P = \frac{1}{3} n < pv >= \frac{1}{3} \int_0^{\infty} n(p) p v(p) dp, \tag{11}$$

where number density as a function of momentum, p, is given by,

$$n(p) = \begin{cases} \frac{8\pi}{h^3} p^2 & \text{if } p < p_F \\ 0 & \text{if } p > p_F, \end{cases} \tag{12}$$

and Fermi momentum, p_F, is given by,

$$n = \frac{8\pi}{h^3} \int_0^{p_F} p^2 dp = \frac{8\pi}{3h^3} p_F^3 \rightarrow p_F = \left[\frac{3h^3}{8\pi} \frac{\rho}{\mu m_u}\right]^{\frac{1}{3}}. \tag{13}$$

For a relativistic gas the energy can be recast in terms of the relativistic gamma factor (different to the function $\gamma(y)$),

$$\left(m_e c^2\right)^2 + (pc)^2 = \gamma^2 (m_e c^2)^2, \tag{14}$$

which can be rearranged for velocity using $\gamma = \frac{1}{\sqrt{1-\left(\frac{v}{c}\right)^2}}$ to give,

$$v(p) = c\left[1 - \frac{1}{1 + \left(\frac{p}{m_e c^2}\right)^2}\right]^{\frac{1}{2}}. \tag{15}$$

Substituting this into (11) at the limit of Fermi momentum gives,

$$P = \frac{1}{3} \int_0^{p_F} \frac{8\pi}{h^3} p^2 p v(p_F) dp. \tag{16}$$

Using chain rule, $\frac{dP}{d\rho} = \frac{dP}{dp}\frac{dp}{d\rho}$ to express this in terms of density yields,

$$\frac{dP}{d\rho} = \frac{8\pi}{3h^3} p_F^3 v(p_F) \frac{dp}{d\rho}\bigg|_{p_F}. \tag{17}$$

Substituting (13), evaluating, and rearranging gives,

$$\frac{dP}{d\rho} = \frac{1}{3}\frac{\rho^{1/3}}{\mu m_u} c \left[\frac{1}{1+\left(\frac{m_e c^2}{p_F}\right)^2}\right]^{\frac{1}{2}} \left[\frac{3h^3}{8\pi}\frac{1}{\mu m_u}\right]^{\frac{1}{3}}. \tag{18}$$

Using the relation $p_F \sim p^{\frac{1}{3}}$, therefore $\frac{p_F}{m_e c^2} \sim \frac{\rho}{\rho_0}^{\frac{1}{3}}$, we arrive at the required form,

$$\frac{dP}{d\rho} = Y_e \frac{m_e c^2}{m_p} \frac{y^{\frac{2}{3}}}{3\left(1 + y^{\frac{2}{3}}\right)^{\frac{1}{2}}}, \tag{19}$$

where $y = \frac{\rho}{\rho_0}$.

Appendix B: Non-Relativistic Case

For the case of a non-relativistic gas model, the velocity becomes the classical $v(p) = \frac{p}{m_e}$, resulting in the following equation for pressure:

$$P = \frac{1}{3}\int_0^{p_F} n(p) \frac{p^2}{m_e} dp. \tag{20}$$

Following the same procedure as for the relativistic case, we arrive at,

$$\frac{dP}{d\rho} = Y_e \frac{m_e c^2}{3m_p} \left(\frac{\rho}{\rho_0}\right)^{\frac{2}{3}}. \tag{21}$$

By similar method as shown in section 2.1, the following can be attained:

$$\boxed{\frac{dM}{dx} = 3x^2 q,} \qquad \text{and} \qquad \boxed{\frac{dq}{dx} = -D\frac{q^{\frac{1}{3}} M}{x^2},} \tag{22}$$

where the constant D is given by,

$$D = \frac{4\pi G R_0^2 \rho_0 m_p}{Y_e m_e c^2}. \tag{23}$$

Appendix C: Extremely-Relativistic Case

For the case of an extremely-relativistic gas model, the velocity becomes the speed of light, $v(p) = c$, resulting in the following equation for pressure:

$$P = \frac{1}{3}\int_0^{p_F} n(p)pcdp, \tag{24}$$

Following the same procedure as for the relativistic case, we arrive at,

$$\frac{dP}{d\rho} = Y_e \frac{m_e c^2}{3m_p}\left(\frac{\rho}{\rho_0}\right)^{\frac{1}{3}} \tag{25}$$

Similarly, the following can be attained:

$$\boxed{\frac{dM}{dx} = 3x^2 q,} \qquad \text{and} \qquad \boxed{\frac{dq}{dx} = -D\frac{q^{\frac{2}{3}}M}{x^2},} \tag{26}$$

Appendix D: Mass-Radius Relation

The method for constructing Fig. 2, the main outcome of this project, is detailed below. An array of core densities ranging from 10^{-4} to 10^{12} is created and cycled through, with the final value where the density tends to zero at the surface being plotted to give the shape in Fig. 2 (with inverted axes). Below is a graphical example of the process for a C core.

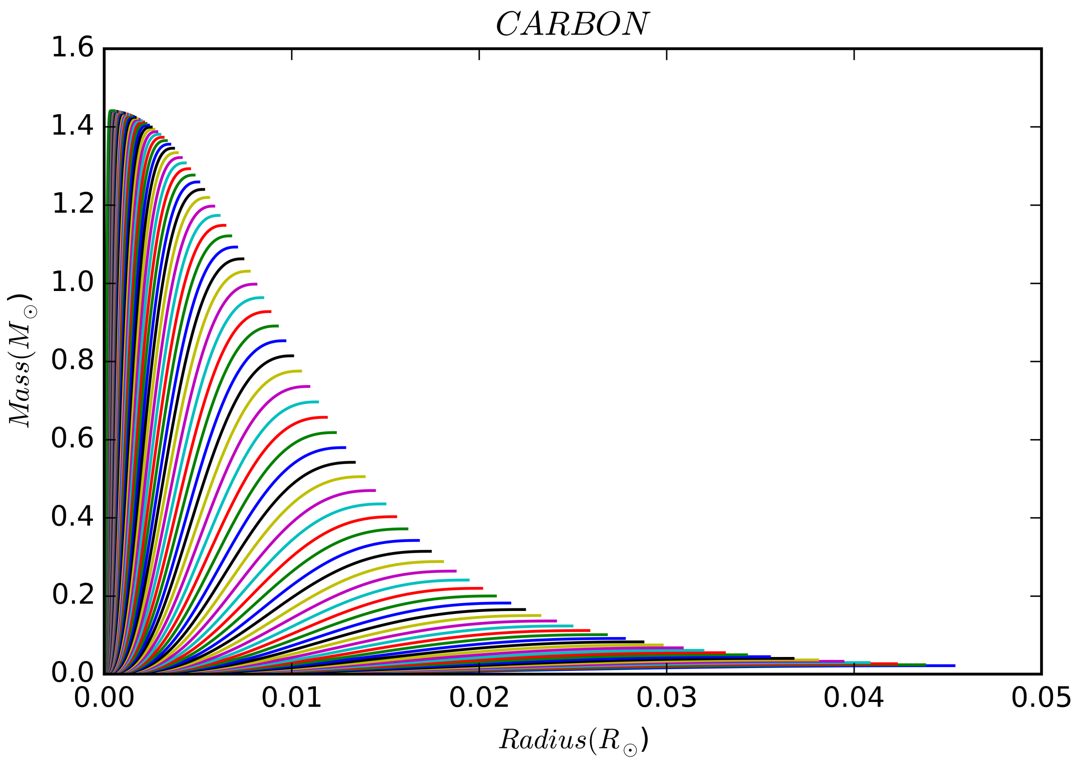

Figure 5: Method for constructing the mass against radius figure. A line is plotted from the end points from each of these core density lines, and axis inverted to give Fig. 2.

References

[1] Fontaine, G. et al. (2013). An overview of white dwarf stars. EPJ Web of Conferences, 43, p.05001.

[2] Barstow, M. and Werner, K. (2006). Structure and Evolution of White Dwarfs and their Interaction with the Local Interstellar Medium. Astrophys Space Sci, 303(1-4), pp.3-16.

[3] Giammichele, N., Bergeron, P. and Dufour, P. (2012). Know Your Neighborhood: A Detailed Model Atmosphere Analysis of Nearby White Dwarfs. ApJS, 199(2), p.29.

[4] Chandrasekhar, S. (1957). An Introduction to the Study of Stellar Structure. (Dover, New York).

[5] Jordan, G., Perets, H., Fisher, R. and van Rossum, D. (2012). Failed-Detonation Supernovae: Subluminous Low-Velocity 1a Supernovae and their Kicked Remnant White Dwarfs with Iron-Rich Cores. ApJ, 761(2), p.L23.

[6] Hawke, I. and Alessandro, G. D. (2015). Numerical Methods MATH3018/6111.

[7] Provencal, J. et al. (2002). Procyon B: Outside the Iron Box. ApJ, 568(1), pp.324-334.

[8] Chandrasekhar, S. (1984). Reviews of Modern Physics, vol 56, page 137

[9] Shapiro, S. and Teukolsky, S. (1983). Black Holes, White Dwarfs, and Neutron Stars. (J Wiley and Sons, Inc., New York 1983) Chapter 3.

[10] Fitzpatrick, R. (29/03/2006). Runge-Kutta methods. [online] Farside.ph.utexas.edu. Available at: http://farside.ph.utexas.edu/teaching/329/lectures/node35.html [Accessed 16 Mar. 2016].

[11] Hu, Q., Wu, C. and Wu, X. (2007). The mass and luminosity functions and the formation rate of DA white dwarfs in the Sloan Digital Sky Survey. Astronomy and Astrophysics, 466(2), pp.627-639.

[12] Dan, M., Rosswog, S., Guillochon, J. and Ramirez-Ruiz, E. (2012). How the merger of two white dwarfs depends on their mass ratio: orbital stability and detonations at contact. Monthly Notices of the Royal Astronomical Society, 422(3), pp.2417-2428.

[13] Hachisu, I., Kato, M. and Nomoto, K. (2012). Final Fates of Rotating White Dwarfs and their Companions in the Single Degenerate Model of Type 1a Supernovae. ApJ, 756(1), p.L4.

[14] Isern, J., Artigas, A. and Garca-Berro, E. (2013). White dwarf cooling sequences and cosmochronology. EPJ Web of Conferences, 43, p.05002.

[15] Pols, O. (2011). Stellar Structure and Evolution. Astronomical Institute Utrecht, Chapters 1-13.